NANO LETTERS
Letter
Cite This: Nano Lett. 2019, 19, 4897−4903
pubs.acs.org/NanoLett

Spontaneous Formation of 1D Pattern in Monolayer VSe_2 with Dispersive Adsorption of Pt Atoms for HER Catalysis

Zhong-Liu Liu,[†,#] Bao Lei,[†,#] Zhi-Li Zhu,[†,#] Lei Tao,[†,//,#] Jing Qi,[†] De-Liang Bao,[†,//] Xu Wu,[†] Li Huang,[†] Yu-Yang Zhang,[†,§] Xiao Lin,[†,§] Ye-Liang Wang,[*,†,‡,§] Shixuan Du,[*,†,§] Sokrates T. Pantelides,[//,†] and Hong-Jun Gao[*,†,§]

[†]Institute of Physics and University of Chinese Academy of Sciences, Chinese Academy of Sciences, Beijing 100190, China
[‡]School of Information and Electronics, Beijing Institute of Technology, Beijing 100081, China
[§]CAS Center for Excellence in Topological Quantum Computation, Beijing 100049, China
[//]Department of Physics and Astronomy, Vanderbilt University, Nashville, Tennessee 37235, United States

Supporting Information

ABSTRACT: Creation of functional patterns in two-dimensional (2D) materials provides opportunities to extend their potential for applications. Transition-metal dichalcogenides (TMDCs) are suitable 2D materials for pattern generation because of properties including alterable polymorphic phases, easy chalcogen-vacancy formation, metal-atom insertion, and alloying. Such patterning can be used for selective functionalization. Here we report the spontaneous formation of long-range, well-ordered 1D patterns in monolayer vanadium diselenide (VSe_2) by a single annealing stage during growth. Atomic-resolution images in real space combined with density-functional-theory (DFT) calculations reveal the 1D features of patterned VSe_2. Further experimental characterization of the intermediate states in the growth process confirm the spontaneous formation of the 1D pattern by annealing-induced Se-deficient linear defects. The 1D pattern can be reversibly transformed to homogenous VSe_2 monolayer by reintroducing Se atoms. Moreover, additional experiments demonstrate that a dispersive deposition of Pt atoms along the 1D structures of patterned VSe_2 is achieved, while DFT calculations find that their catalytic activity for hydrogen evolution reaction (HER) is as good as that of Pt surfaces. The formation of long-range, well-ordered 1D patterns not only demonstrates an effective way of dimension modulation in 2D materials but also enriches the potential of intrinsically patterned 2D materials for promising catalytic activities.

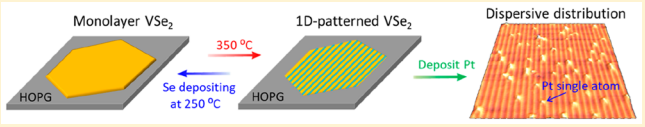

KEYWORDS: *VSe_2, one-dimensional pattern, two-dimensional materials, reversible transformation, dispersive adsorption, single atom catalysts*

Functionalization of two-dimensional (2D) materials has a significant impact on their intriguing properties, immensely expanding their application potential in electronics,[1,2] optics,[3,4] chemistry,[5] energy,[6] and biomedicine.[7,8] As a widely used method to functionalize 2D materials, formation of geometric patterns in 2D materials provide not only an extra dimension to manipulate their atomic structures and properties in the nanoscale but also new platforms to combine with other processes for multiple applications. Patterning of 2D materials by extrinsic means such as electron-beam,[9] focused-ion-beam,[10] incorporation of excess metal atoms,[11] or lithography[12,13] has been reported. Patterning has led to the functionalization of various 2D systems with novel properties, such as semiconducting nanomesh-like graphene,[14] laser-induced phase patterning of $MoTe_2$[15] for Ohmic contacts, photoluminescence in nanopatterned MoS_2,[16] and selective adsorption of functional molecules on intrinsically patterned $PtSe_2$ or CuSe.[17]

Among hundreds of 2D materials, transition-metal dichalcogenides (TMDCs) with an MX_2 formula have great advantages for pattern formation. TMDCs have a typical sandwich-layered structure with different polymorphic phases[18] (e.g. 2H, 1T) that provide a convenient platform to fabricate patterns by phase manipulation. Moreover, the ease of chalcogen-vacancy formation and metal-atom insertion in an otherwise stable sandwich-layered structure are additional degrees of freedom that have been exploited to generate unique patterns by judiciously chosen annealing steps[9,11,17,19] or even to fuse two monolayers into a new monolayer structure.[20] Pattern generation offers unique opportunities for selective, even dual functionalization for catalysis, sensing, or other applications.[17] The objective of combining patterning with functionalization is emerging as a promising frontier.

Vanadium diselenide (VSe_2) is a member of the TMDC family of 2D materials with a typical sandwich T-phase structure and its own unique and diverse properties[18] which have generated widespread interest. Specifically, intrinsic monolayer (ML) VSe_2 exhibits 2D ferromagnetism,[21,22]

Received: March 2, 2019
Revised: April 9, 2019
Published: April 11, 2019

DOI: 10.1021/acs.nanolett.9b00889
Nano Lett. 2019, 19, 4897−4903

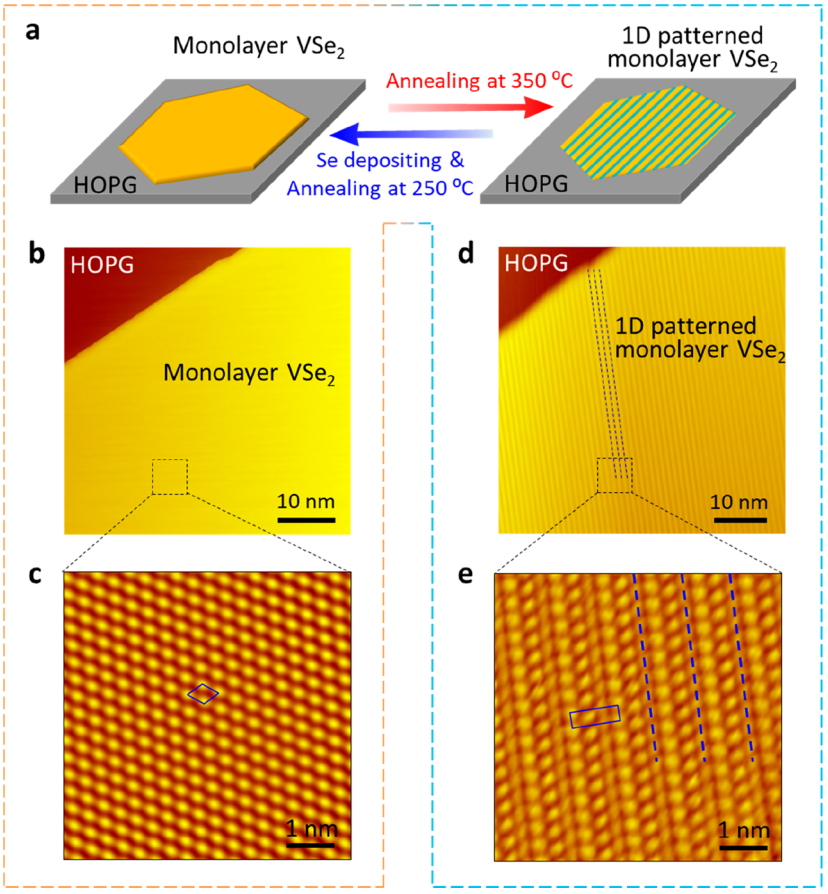

Figure 1. Reversible transformation between homogeneous ML VSe_2 and 1D-patterned ML VSe_2. (a) Schematic of the reversible transformation. (b) STM topographic image (−2.0 V, 0.1 nA) of homogeneous ML VSe_2 on HOPG. (c) Atomic-resolution STM image (−1.0 V, 0.8 nA) of ML VSe_2 showing a hexagonal lattice with a periodicity of 0.33 nm. The unit cell is depicted by the blue rhombus. (d) STM topographic image (−2.0 V, 0.1 nA) of 1D-patterned ML VSe_2 on HOPG. The 1D pattern is highlighted by blue dashed lines. (e) Atomic-resolution STM image (−1.0 V, 0.8 nA) of 1D-patterned ML VSe_2 shows its rectangular lattice, whose unit cell is depicted by the blue rectangle. The lattice parameters are 0.97 and 0.34 nm, respectively. The blue dashed lines highlight the 1D pattern.

extra-high conductivity,[23] excellent electrocatalysis,[24] and a charge-density-wave (CDW) transition.[25,26] In this Letter, we demonstrate spontaneous formation of well-ordered 1D patterns in ML VSe_2 by a single annealing stage during growth. Periodic 1D-patterned structures with a period about 1 nm form on as-grown homogeneous ML VSe_2 on a highly oriented pyrolytic graphite (HOPG) substrate when it is annealed to about 350 °C. The 1D-patterned VSe_2 can be transformed to the original homogeneous ML VSe_2 by introducing Se atoms at a lower sample temperature of 250 °C. The structure of the 1D patterning is confirmed by atomic-resolution scanning tunneling microscopy (STM) and atomic-force microscopy (AFM) combined with density-functional-theory (DFT) calculations, revealing that the generation of 1D patterning in the ML VSe_2 is undergirded by Se-deficient linear defects. Further STM characterization of intermediate states reveals the transformation process from homogeneous ML VSe_2 to 1D-patterned ML VSe_2. Selenium-deficient linear defects are produced and increase in number as the VSe_2 sample is annealed. The density of these linear defects finally reaches a limit that results in periodic arrays of 1D structures. Finally, platinum (Pt) deposition experiments show that the Pt atoms are selectively adsorbed on the 1D structures of patterned VSe_2, mostly in a monodispersed fashion with roughly 30% forming pairs. DFT calculations then demonstrate that monodispersed Pt atoms are as good as Pt surfaces for hydrogen evolution reaction (HER) catalysis, while Pt pairs and 50%-occupied 1D structures are nearly as good.

Homogeneous ML VSe_2 was fabricated on an HOPG substrate in an ultrahigh vacuum (UHV) chamber by co-evaporation of Se and V atoms[22] while annealing at 270 °C (see Sample Preparation). When the as-grown sample is annealed to 350 °C, homogeneous VSe_2 transforms to a 1D-patterned structure. When selenium is evaporated on the 1D-patterned ML VSe_2 while annealing at 250 °C, the ML recovers its original homogeneous state. Figure 1a shows a schematic representation of the experimental process for the reversible transformation between intrinsic ML VSe_2 and 1D-patterned ML VSe_2.

Panels b and c of Figure 1 are typical STM images of the homogeneous-phase ML VSe_2. The atomic-resolution image in Figure 1c demonstrates an atomically smooth flat monolayer with a well-ordered hexagonal lattice. The primitive unit cell of this lattice is illustrated by a blue rhombus, each of whose sides is 0.33 nm. After annealing, the samples exhibit a 1D linear pattern illustrated by blue dashed-lines in the STM images in Figures 1d and 1e. It is particularly intriguing that the lattice structure changes from a hexagonal to a rectangular Bravais lattice. The primitive unit cell of the rectangular lattice is

DOI: 10.1021/acs.nanolett.9b00889
Nano Lett. 2019, 19, 4897−4903

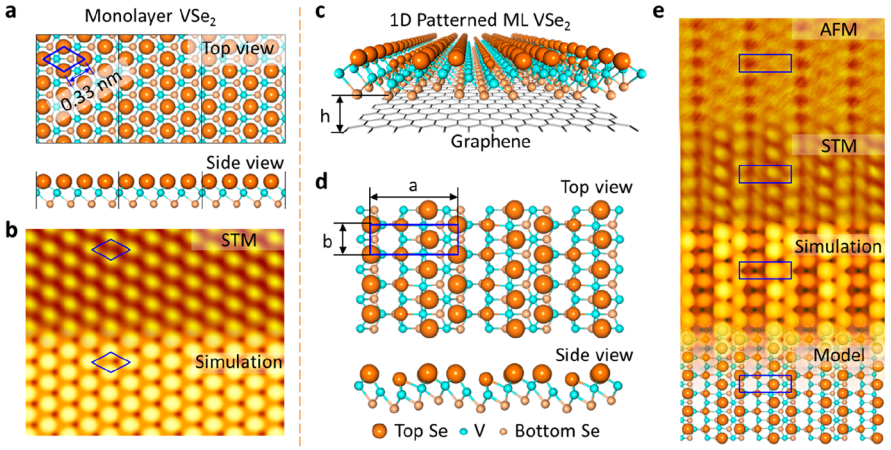

Figure 2. Structure model and DFT simulations of homogenous and 1D-patterned ML VSe_2. (a) Top view and side view of the atomic structure of homogeneous ML VSe_2. The Se atoms on top and bottom are shown in different size balls for better discrimination. The blue rhombus depicts the unit cell. Both the top view and side view are equidistantly divided by black lines for comparison with the 1D-patterned phase. (b) STM image (upper) and simulation (lower) of homogeneous ML VSe_2. The blue rhombus depicts the unit cell. (c) Structural model of 1D-patterned ML VSe_2 on graphene obtained by DFT calculations. The calculated distance between the graphene and the bottom Se atoms is 0.33 nm. (d) Top view and side view of the structural model of 1D-patterned phase. The top Se atoms are shown in different size balls to exhibit the undulating height. The blue rectangle depicts the unit cell, whose calculated length and width are a = 0.99 nm, b = 0.34 nm. (e) AFM attractive-force image, atomic-resolution STM image, simulated STM image, and structural model of 1D-patterned ML VSe_2 match each other.

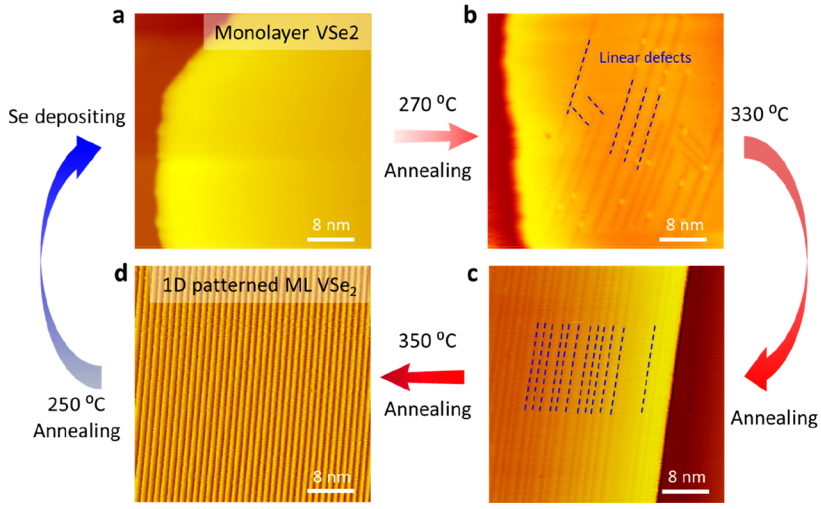

Figure 3. Transformation process between homogeneous VSe_2 and 1D-patterned ML VSe_2. (a) STM image of ML VSe_2 on HOPG. (b) STM image from the same sample in (a) after annealing to 270 °C. The blue-dashed lines indicate the linear defects with different orientations. (c,d) STM images from the same sample as in (b) after annealing to 330 °C and 350 °C, respectively. The blue-dashed lines highlight the 1D pattern. All images are obtained with the scanning parameter (−2.0 V, 0.1 nA).

indicated by a blue rectangle in Figure 1e. This rectangle is 0.97 nm along its long axis and 0.34 nm along its short axis.

To figure out the precise atomic structure of the 1D pattern, we constructed atomic models for both the homogeneous and the 1D-patterned phases, relaxed the models by DFT calculations, and simulated the models' STM images for comparison with the experimental STM images. The homogeneous-phase model is shown in Figure 2a, while the corresponding simulated STM image and the experimental STM image of the homogeneous phase are compared in Figure 2b. Since the 1D-patterned phase is formed by annealing and the homogeneous phase can be recovered by selenium deposition in this reversible transformation process, the 1D pattern should be a Se-deficient structure compared to the structure of the original homogenous VSe_2. We constructed a Se-deficient model for the 1D pattern as shown in Figure 2c. In this model, one row of top selenium atoms is removed from each group of four adjacent rows along the long axis of the rectangular unit cell so that the surface Se atoms form an undulating linear pattern, as seen clearly in the side view in Figure 2d. According to the lowest-energy relaxed model, the rectangular unit cell is 0.99 nm along its long axis and 0.34 nm along its short axis, which are in excellent agreement with the experimental values of 0.97 and 0.34 nm, respectively. The simulated STM image based on this relaxed structure also matches well the experimental STM image, as shown in Figure 2e.

We have also carried out AFM characterization of the sample to further confirm the 1D pattern structure and eliminate possible influence of the local electronic states to the topography of the sample in STM measurements. In an attractive-force image obtained in the non-contact mode of

DOI: 10.1021/acs.nanolett.9b00889
Nano Lett. 2019, 19, 4897−4903

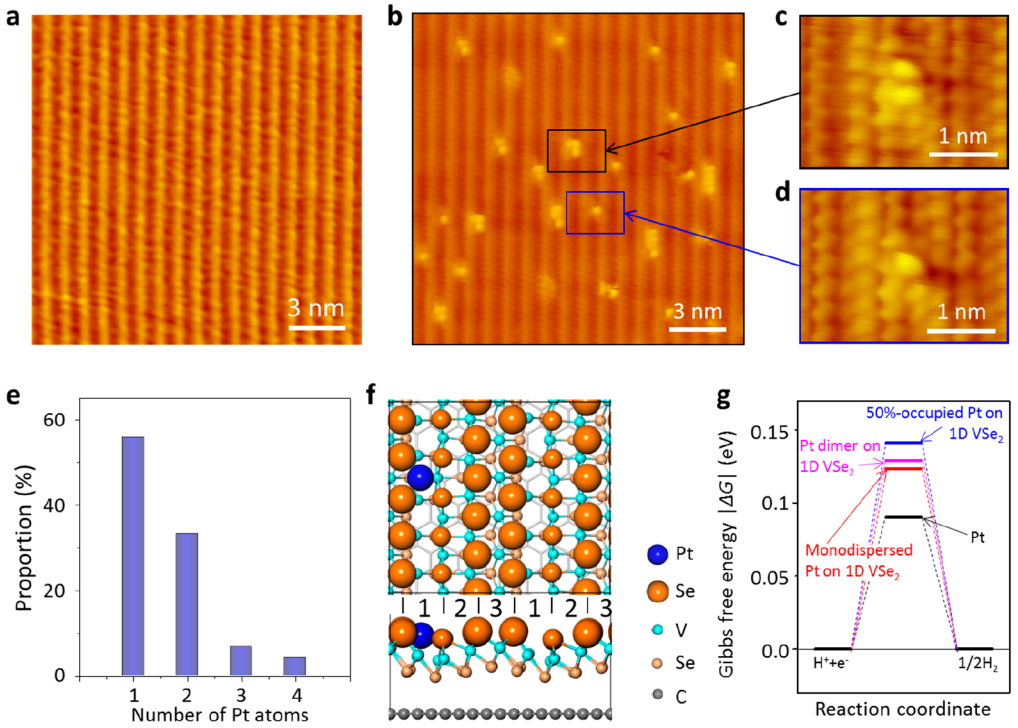

Figure 4. Pt adatoms on 1D-patterned ML VSe_2. (a) STM image (−2.0 V, 0.3 nA) of 1D-patterned ML VSe_2 on HOPG before Pt deposition. (b) STM image (−2.0 V, 0.3 nA) of the same sample in (a) after Pt deposition. The bright dots are the adsorbed Pt adatoms. (c,d) Zoom-in STM images (−1.0 V, 0.8 nA) of adsorbed Pt dimer and single atom, respectively. (e) Statistical distribution of Pt adatoms adsorbed on 1D-patterned ML VSe_2. (f) Atomic models of single Pt adatom on 1D-patterned ML VSe_2. (g) Calculated absolute value of the Gibbs free energy for atomic hydrogen adsorption ($|\Delta G_H|$) on Pt adatoms in different configurations comparing with the $|\Delta G_H|$ on pure Pt. 50%-occupation means that, in the unit cell shown in (f), the left channel 1 is fully occupied, leaving the right channel 1 empty (see Figure S4).

AFM, shown in the top part of Figure 2e, there are rows of distinct hollow sites along the Se-deficient rows of the model, seen as dark holes, where the attractive force is weaker due to the relatively larger distance from the tip to the local atoms. On the basis of the combined data from STM, AFM, and DFT methods, which is consistent with each other, we confirmed that the model we propose represents the real structure of 1D-patterned ML VSe_2.

After the structure of the 1D-patterned phase was confirmed, the formation process of this phase was further investigated by STM characterization of the intermediate states in the transformation from the homogeneous phase. Figure 3 show the whole process of the reversible transformation between ML VSe_2 and 1D-patterned ML VSe_2. Figure 3a is the STM image obtained on a homogeneous ML VSe_2 on HOPG substrate. When the sample is annealed to 270 °C, linear defects emerge on the ML VSe_2 (Figure 3b), as it loses selenium atoms. The linear defects in a continuous VSe_2 island have three orientations with 60° angle to each other due to the VSe_2 symmetry. These linear defects are distributed more randomly and have a lower density compared with those in well-ordered 1D-patterned VSe_2. As the sample is annealed to a higher sample temperature of 330 °C, the density of the linear defects increases, and the linear defects align much more regularly, parallel to each other in each rotational domain. Yet the intervals between these linear defects are still varying (Figure 3c), that is, their density has not reached a limit. When the annealing temperature of the sample increases to 350 °C, the density of linear defects finally reaches its limit. The homogeneous ML VSe_2 phase is completely transformed to the 1D-patterned ML VSe_2 phase in which the linear defects align regularly with a uniform interval (Figure 3d).

Because the transformation to 1D-patterned ML VSe_2 is driven by a deficiency of selenium atoms, it should be reversible by reintroducing selenium. It is confirmed by our experiments that when selenium is deposited on the 1D-patterned ML VSe_2 while the sample is kept at a lower temperature, 250 °C, the 1D-patterned ML VSe_2 can be restored to homogeneous VSe_2. This transformation, therefore, proves that removal of selenium atoms is the key to the original transformation of homogeneous ML VSe_2 to 1D-patterned ML VSe_2. For more details of this reversible transformation with more intermediate steps, see Figure S1 in the Supporting Information. The statistical analysis of linear defects in monolayer VSe_2 sample annealing at different temperatures is shown in Figure S2.

Single-atom catalysts (SAC) with individual and isolated metal atoms such as Pt, anchored to supports, possess high efficiency in heterogeneous reactions.[27−30] Two-dimensional materials such as graphene,[31] nitrogen-doped graphene,[32,33] and MoS_2,[34] which have large surface-area, have been predicted to be very good supports for SAC. The undulating pattern shaped by periodic linear defects, as seen in the side view of Figure 1d, makes the 1D-patterned ML VSe_2 a suitable template for selective adsorption of Pt adatoms. We deposited Pt atoms onto the pre-fabricated 1D-patterned ML VSe_2. Figures 4a and 4b show STM images of the sample before and after the deposition of the Pt atoms, respectively. Figure 4b demonstrates that the Pt adatoms are adsorbed in a dispersed fashion (see also Figure S3). The atomic-resolution STM images in Figure 4c,d, show clearly that Pt atoms and Pt dimers

DOI: 10.1021/acs.nanolett.9b00889
Nano Lett. 2019, 19, 4897−4903

are adsorbed in the Se-deficient channels. The adsorbed Pt atoms are mostly single, isolated atoms, with a fair number of pairs and a few trimers and tetramers (Figure S4). The statistical distribution obtained from STM images measured at different positions of the sample (Figure S3) is shown in Figure 4e. The above observations reveal that 1D-patterned ML VSe_2 can be a promising candidate platform for the fabrication of single-Pt-atom catalyst.

To better understand the adsorption structure of Pt adatoms on 1D-patterned ML VSe_2, we carried out DFT calculations. Considering that one of each four rows of top-layer Se atoms are gone, there are three different kinds of channels for Pt adatoms to be adsorbed in, as depicted by 1, 2, and 3 in Figure 4f. DFT calculations (Figure S5) show that single-Pt adatom located in channel 1 (the Se-deficient channel) is the most stable structure, as shown in Figure 4e, which is in agreement with the experimental results. DFT calculations further confirm that disperse adsorption of Pt adatoms on 1D-patterned ML VSe_2 is more energetically favorable. As shown in Figure S6, the adsorption energy per Pt atom is the largest for isolated Pt atoms than for any other configuration we are able to study, including the 50%-occupied 1D structures. Computational limitations on supercell size do not allow us to calculate accurately the binding energy of isolated pairs, but we do find that pair formation is not energetically favored when other Pt atoms are in proximity (as is the case in our relatively small supercells). This result suggests that the concentration of deposited Pt atoms can be tuned to achieve monodispersed adsorption. It is also notable that Pt adatoms can occupy the whole channel at 50% occupancy with an adsorption energy of −5.5 eV/Pt, forming a very stable structure.

After the structural stability of adsorbed Pt adatoms was investigated, we checked the reaction activity for HER of Pt atoms on the 1D-patterned VSe_2. We find that the atomic-level dispersed Pt atoms on 1D-patterned ML VSe_2 is a promising SAC for HER. Figure 4g shows the absolute value of the Gibbs free energy ($|\Delta G_H|$) of Pt adatoms in different configurations for HER. For a single Pt atom on a 1D-patterned VSe_2 (Figure 4f), the $|\Delta G_H|$ value is 0.12 eV, followed by a Pt dimer of 0.13 eV. When the Se-deficient channels of the 1D-patterned VSe_2 is 50%-occupied by Pt atoms, $|\Delta G_H|$ is 0.14 eV, that is, also indicating good catalytic activity for HER. Compared to Pt bulk surfaces, which is the best cathode material for HER with a calculated $|\Delta G_H|$ of 0.09 eV,[35] the DFT calculations demonstrate the excellent catalytic activity of Pt adatoms on 1D-patterned VSe_2. Thus, the 1D-patterned VSe_2 shows great potential as a support material in SAC.

In summary, we discovered a reversible transformation between ML VSe_2 and 1D-patterned ML VSe_2. The structure of the 1D-patterned ML VSe_2 is revealed, and the mechanism of the transformation is investigated. We further explored the dispersive adsorption of Pt atoms on the 1D-pattern and predict its catalytic activities. Such formation of long-range well-ordered 1D-pattern in ML VSe_2 not only demonstrates dimension modulation in 2D materials, but also exhibits promising potential of functionalized 2D materials like HER applications.

Methods. *Sample Preparation.* ML VSe_2 was fabricated on an HOPG substrate in an ultrahigh vacuum (UHV) chamber, with a base pressure of 2×10^{-10} mbar, equipped with standard MBE capabilities. The HOPG substrate was cleaved and annealed to 1100 K in the UHV chamber. Selenium atoms (Sigma, 99.999%) were evaporated from a Knudsen cell, and vanadium atoms (ESPI Metals, 99.999%) were evaporated from an electron-beam evaporator and deposited onto the substrate, which was annealing at 270 °C during the deposition. The coverage of ML VSe_2 can be controlled by the growth time and fluxes of atoms. By annealing the sample at 350 °C, the ML VSe_2 transforms to 1D-patterned ML VSe_2. Additionally, by depositing selenium atoms and keeping the sample at 250 °C, the 1D-patterned ML VSe_2 can be recovered to the original homogeneous ML VSe_2. For adsorption of Pt adatoms, Pt atoms (ESPI Metals, 99.999%) were evaporated from an electron-beam evaporator and deposited on the 1D-patterned ML VSe_2 at room temperature.

Sample Characterization. STM measurements were performed in an UHV STM-LEED combined system with a base pressure of 3.0×10^{-10} mbar. All the STM images of the samples were acquired in the constant-current mode, using an electrochemically etched tungsten tip. The bias voltages were applied to the sample with respect to the tip. The Nanotec Electronica WSxM software was used to process the STM images. AFM Measurements was conducted in an UHV low-temperature AFM system. All the AFM images were acquired with an electrochemically etched tungsten tip in the non-contact mode at 4.5 K.

DFT Calculations. DFT calculations based on density functional theory (DFT) are performed using the Vienna Ab initio Simulation Package[36,37] (VASP). The projector augmented wave[38] (PAW) method is employed, and the Perdew−Burke−Ernzerhof (PBE) version of the generalized gradient approximation[39] (GGA) was used. The electronic wavefunctions are expanded in plane waves with a kinetic energy cutoff of 500 eV. For freestanding VSe_2 structure, the *k*-points sampling is 25 × 25 × 1, generated automatically with the origin at the Γ-point. For 1D-patterned VSe_2 on HOPG, the *k*-points sampling is with only the Γ-point. The structures were relaxed until the energy and residual force on each atom were smaller than 10^{-6} eV and 0.01 eV/Å, respectively. The vacuum layers of the two models are larger than 20 Å. The STM simulations are performed using the Tersoff-Hamann approach.[40] The Gibbs free energy of hydrogen adsorption, ΔG_H, is calculated as $\Delta G_H = \Delta E_H + \Delta E_{ZPE} - T\Delta S_H$. ΔE_H is the binding energy of adsorbed hydrogen. ΔE_{ZPE} and ΔS_H are the zero-point energy difference and entropy difference between the adsorbed hydrogen and hydrogen in the gas phase, respectively. In the standard condition, $\Delta E_{ZPE} - T\Delta S_H$ is approximately 0.24 eV, which is a widely accepted value.[35]

■ ASSOCIATED CONTENT

Supporting Information

The Supporting Information is available free of charge on the ACS Publications website at DOI: 10.1021/acs.nanolett.9b00889.

Details of the reversible transformation process between ML VSe_2 and 1D-patterned ML VSe_2, statistics of 1D pattern formation in ML VSe_2 sample annealing at different temperatures, STM images measured at different positions of the sample, profile measurements of a Pt tetramer adsorbed on 1D-patterned VSe_2, DFT calculations of the selective adsorption of Pt atoms on 1D-patterned ML VSe_2 (PDF)

DOI: 10.1021/acs.nanolett.9b00889
Nano Lett. 2019, 19, 4897−4903

AUTHOR INFORMATION

Corresponding Authors

*E-mail for Y.L.W.: ylwang@iphy.ac.cn. Fax: 0086-10-62556598.
*E-mail for S.X.D.: sxdu@iphy.ac.cn.
*E-mail for H.J.G.: hjgao@iphy.ac.cn.

ORCID

De-Liang Bao: 0000-0002-5070-4765
Yu-Yang Zhang: 0000-0002-9548-0021
Ye-Liang Wang: 0000-0002-8896-0748
Shixuan Du: 0000-0001-9323-1307
Hong-Jun Gao: 0000-0002-6766-0623

Author Contributions

#These authors (Z.L.L., B.L., Z.L.Z., and L.T.) contributed equally to this work.

Notes

The authors declare no competing financial interest.

ACKNOWLEDGMENTS

We acknowledge financial support from the National Key Research & Development Projects of China (2016YFA0202300), National Natural Science Foundation of China (Nos. 61725107, 51572290, 61888102, 51872284), Strategic Priority Research Program of the Chinese Academy of Sciences (Grant Nos. XDB30000000 and XDB28000000). Work at Vanderbilt University (S.T.P., D.L.B.) was supported in part by the U.S. Department of Energy grant DE-FG02-09ER46554 and by the McMinn Endowment. Computational resources were provided by the National Supercomputing Center in Tianjin.

REFERENCES

(1) Fiori, G.; Bonaccorso, F.; Iannaccone, G.; Palacios, T.; Neumaier, D.; Seabaugh, A.; Banerjee, S. K.; Colombo, L. Electronics based on two-dimensional materials. *Nat. Nanotechnol.* **2014**, *9* (10), 768−779.

(2) Jariwala, D.; Sangwan, V. K.; Lauhon, L. J.; Marks, T. J.; Hersam, M. C. Emerging Device Applications for Semiconducting Two-Dimensional Transition Metal Dichalcogenides. *ACS Nano* **2014**, *8* (2), 1102−1120.

(3) Ross, J. S.; Rivera, P.; Schaibley, J.; Lee-Wong, E.; Yu, H. Y.; Taniguchi, T.; Watanabe, K.; Yan, J. Q.; Mandrus, D.; Cobden, D.; Yao, W.; Xu, X. D. Interlayer exciton optoelectronics in a 2D heterostructure p−n junction. *Nano Lett.* **2017**, *17* (2), 638−643.

(4) Miller, O. D.; Ilic, O.; Christensen, T.; Reid, M. T. H.; Atwater, H. A.; Joannopoulos, J. D.; Soljacic, M.; Johnson, S. G. Limits to the optical response of graphene and two-dimensional materials. *Nano Lett.* **2017**, *17* (9), 5408−5415.

(5) Chhowalla, M.; Shin, H. S.; Eda, G.; Li, L. J.; Loh, K. P.; Zhang, H. The chemistry of two-dimensional layered transition metal dichalcogenide nanosheets. *Nat. Chem.* **2013**, *5* (4), 263−275.

(6) Mendoza-Sanchez, B.; Gogotsi, Y. Synthesis of Two-Dimensional Materials for Capacitive Energy Storage. *Adv. Mater.* **2016**, *28* (29), 6104−6135.

(7) Kurapati, R.; Kostarelos, K.; Prato, M.; Bianco, A. Biomedical Uses for 2D Materials Beyond Graphene: Current Advances and Challenges Ahead. *Adv. Mater.* **2016**, *28* (29), 6052−6074.

(8) Kenry; Chaudhuri, P. K.; Loh, K. P.; Lim, C. T. Selective Accelerated Proliferation of Malignant Breast Cancer Cells on Planar Graphene Oxide Films. *ACS Nano* **2016**, *10* (3), 3424−3434.

(9) Lin, J. H.; Pantelides, S. T.; Zhou, W. Vacancy-induced formation and growth of inversion domains in transition-metal dichalcogenide monolayer. *ACS Nano* **2015**, *9* (5), 5189−5197.

(10) Celebi, K.; Buchheim, J.; Wyss, R. M.; Droudian, A.; Gasser, P.; Shorubalko, I.; Kye, J. I.; Lee, C.; Park, H. G. Ultimate permeation across atomically thin porous graphene. *Science* **2014**, *344* (6181), 289−292.

(11) Coelho, P. M.; Komsa, H. P.; Diaz, H. C.; Ma, Y. J.; Krasheninnikov, A. V.; Batzill, M. Post-synthesis modifications of two-dimensional $MoSe_2$ or $MoTe_2$ by incorporation of excess metal atoms into the crystal structure. *ACS Nano* **2018**, *12* (4), 3975−3984.

(12) Liu, W.; Jackson, B. L.; Zhu, J.; Miao, C. Q.; Chung, C. H.; Park, Y. J.; Sun, K.; Woo, J.; Xie, Y. H. Large scale pattern graphene electrode for high performance in transparent organic single crystal field-effect transistors. *ACS Nano* **2010**, *4* (7), 3927−3932.

(13) Jung, M. W.; Myung, S.; Song, W.; Kang, M. A.; Kim, S. H.; Yang, C. S.; Lee, S. S.; Lim, J.; Park, C. Y.; Lee, J. O.; An, K. S. Novel fabrication of flexible graphene-based chemical sensors with heaters using soft lithographic patterning method. *ACS Appl. Mater. Interfaces* **2014**, *6* (16), 13319−13323.

(14) Bai, J. W.; Zhong, X.; Jiang, S.; Huang, Y.; Duan, X. F. Graphene nanomesh. *Nat. Nanotechnol.* **2010**, *5* (3), 190−194.

(15) Cho, S.; Kim, S.; Kim, J. H.; Zhao, J.; Seok, J.; Keum, D. H.; Baik, J.; Choe, D. H.; Chang, K. J.; Suenaga, K.; Kim, S. W.; Lee, Y. H.; Yang, H. Phase patterning for ohmic homojunction contact in $MoTe_2$. *Science* **2015**, *349* (6248), 625−628.

(16) Han, G. G. D.; Tu, K. H.; Niroui, F.; Xu, W. S.; Zhou, S.; Wang, X. C.; Bulovic, V.; Ross, C. A.; Warner, J. H.; Grossman, J. C. Photoluminescent arrays of nanopatterned monolayer MoS_2. *Adv. Funct. Mater.* **2017**, *27* (45), 1703688.

(17) Lin, X.; Lu, J. C.; Shao, Y.; Zhang, Y. Y.; Wu, X.; Pan, J. B.; Gao, L.; Zhu, S. Y.; Qian, K.; Zhang, Y. F.; Bao, D. L.; Li, L. F.; Wang, Y. Q.; Liu, Z. L.; Sun, J. T.; Lei, T.; Liu, C.; Wang, J. O.; Ibrahim, K.; Leonard, D. N.; Zhou, W.; Guo, H. M.; Wang, Y. L.; Du, S. X.; Pantelides, S. T.; Gao, H. J. Intrinsically patterned two-dimensional materials for selective adsorption of molecules and nanoclusters. *Nat. Mater.* **2017**, *16* (7), 717−721.

(18) Manzeli, S.; Ovchinnikov, D.; Pasquier, D.; Yazyev, O. V.; Kis, A. 2D transition metal dichalcogenides. *Nat. Rev. Mater.* **2017**, *2* (8), 17033.

(19) Arnold, F.; Stan, R. M.; Mahatha, S. K.; Lund, H. E.; Curcio, D.; Dendzik, M.; Bana, H.; Travaglia, E.; Bignardi, L.; Lacovig, P.; Lizzit, D.; Li, Z. S.; Bianchi, M.; Miwa, J. A.; Bremholm, M.; Lizzit, S.; Hofmann, P.; Sanders, C. E. Novel single-layer vanadium sulphide phases. *2D Mater.* **2018**, *5* (4), 045009.

(20) Lin, J. H.; Zuluaga, S.; Yu, P.; Liu, Z.; Pantelides, T.; Suenaga, K. Novel Pd_2Se_3 Two-Dimensional Phase Driven by Interlayer Fusion in Layered $PdSe_2$. *Phys. Rev. Lett.* **2017**, *119* (1), 016101.

(21) Bonilla, M.; Kolekar, S.; Ma, Y. J.; Diaz, H. C.; Kalappattil, V.; Das, R.; Eggers, T.; Gutierrez, H. R.; Phan, M. H.; Batzill, M. Strong room-temperature ferromagnetism in VSe_2 monolayers on van der Waals substrates. *Nat. Nanotechnol.* **2018**, *13* (4), 289−293.

(22) Liu, Z. L.; Wu, X.; Shao, Y.; Qi, J.; Cao, Y.; Huang, L.; Liu, C.; Wang, J. O.; Zheng, Q.; Zhu, Z. L.; Ibrahim, K.; Wang, Y. L.; Gao, H. J. Epitaxially grown monolayer VSe_2: an air-stable magnetic two-dimensional material with low work function at edges. *Sci. Bull.* **2018**, *63* (7), 419−425.

(23) Zhang, Z.; Niu, J.; Yang, P.; Gong, Y.; Ji, Q.; Shi, J.; Fang, Q.; Jiang, S.; Li, H.; Zhou, X.; Gu, L.; Wu, X.; Zhang, Y. Van der Waals epitaxial growth of 2D metallic vanadium diselenide single crystals and their extra-high electrical conductivity. *Adv. Mater.* **2017**, *29* (37), 1702359.

(24) Zhao, W.; Dong, B.; Guo, Z.; Su, G.; Gao, R.; Wang, W.; Cao, L. Colloidal synthesis of VSe2 single-layer nanosheets as novel electrocatalysts for the hydrogen evolution reaction. *Chem. Commun.* **2016**, *52* (59), 9228−9231.

(25) Duvjir, G.; Choi, B. K.; Jang, I.; Ulstrup, S.; Kang, S.; Thi Ly, T.; Kim, S.; Choi, Y. H.; Jozwiak, C.; Bostwick, A.; Rotenberg, E.; Park, J. G.; Sankar, R.; Kim, K. S.; Kim, J.; Chang, Y. J. Emergence of a metal-insulator transition and high-temperature charge-density waves in VSe_2 at the monolayer limit. *Nano Lett.* **2018**, *18* (9), 5432−5438.

DOI: 10.1021/acs.nanolett.9b00889
Nano Lett. 2019, 19, 4897−4903

(26) Ryu, H.; Chen, Y.; Kim, H.; Tsai, H. Z.; Tang, S. J.; Jiang, J.; Liou, F.; Kahn, S.; Jia, C. H.; Omrani, A. A.; Shim, J. H.; Hussain, Z.; Shen, Z. X.; Kim, K.; Min, B. I.; Hwang, C.; Crommie, M. F.; Mo, S. K. Persistent charge-density-wave order in single-layer $TaSe_2$. *Nano Lett.* **2018**, *18* (2), 689−694.
(27) Qiao, B. T.; Wang, A. Q.; Yang, X. F.; Allard, L. F.; Jiang, Z.; Cui, Y. T.; Liu, J. Y.; Li, J.; Zhang, T. Single-atom catalysis of CO oxidation using Pt-1/FeO_x. *Nat. Chem.* **2011**, *3* (8), 634−641.
(28) Tierney, H. L.; Baber, A. E.; Kitchin, J. R.; Sykes, E. C. H. Hydrogen dissociation and spillover on individual isolated palladium atoms. *Phys. Rev. Lett.* **2009**, *103* (24), 246102.
(29) Sohlberg, K.; Rashkeev, S.; Borisevich, A. Y.; Pennycook, S. J.; Pantelides, S. T. Origin of anomalous Pt-Pt distances in the Pt/alumina catalytic system. *ChemPhysChem* **2004**, *5* (12), 1893−1897.
(30) Rashkeev, S. N.; Sohlberg, K.; Glazoff, M. V.; Novak, J.; Pennycook, S. J.; Pantelides, S. T. Transition metal atoms on different alumina phases: The role of subsurface sites on catalytic activity. *Phys. Rev. B: Condens. Matter Mater. Phys.* **2003**, *67* (11), 115414.
(31) Sun, S. H.; Zhang, G. X.; Gauquelin, N.; Chen, N.; Zhou, J. G.; Yang, S. L.; Chen, W. F.; Meng, X. B.; Geng, D. S.; Banis, M. N.; Li, R. Y.; Ye, S. Y.; Knights, S.; Botton, G. A.; Sham, T. K.; Sun, X. L. Single-atom catalysis using Pt/graphene achieved through atomic layer deposition. *Sci. Rep.* **2013**, *3*, 1775.
(32) Zhu, Y. Q.; Cao, T.; Cao, C. B.; Luo, J.; Chen, W. X.; Zheng, L. R.; Dong, J. C.; Zhang, J.; Han, Y. H.; Li, Z.; Chen, C.; Peng, Q.; Wang, D. S.; Li, Y. D. One-pot pyrolysis to N-doped graphene with high-density Pt single atomic sites as heterogeneous catalyst for alkene hydrosilylation. *ACS Catal.* **2018**, *8* (11), 10004−10011.
(33) Cheng, N. C.; Stambula, S.; Wang, D.; Banis, M. N.; Liu, J.; Riese, A.; Xiao, B. W.; Li, R. Y.; Sham, T. K.; Liu, L. M.; Botton, G. A.; Sun, X. L. Platinum single-atom and cluster catalysis of the hydrogen evolution reaction. *Nat. Commun.* **2016**, *7*, 13638.
(34) Deng, J.; Li, H. B.; Xiao, J. P.; Tu, Y. C.; Deng, D. H.; Yang, H. X.; Tian, H. F.; Li, J. Q.; Ren, P. J.; Bao, X. H. Triggering the electrocatalytic hydrogen evolution activity of the inert two-dimensional MoS_2 surface via single-atom metal doping. *Energy Environ. Sci.* **2015**, *8* (5), 1594−1601.
(35) Norskov, J. K.; Bligaard, T.; Logadottir, A.; Kitchin, J. R.; Chen, J. G.; Pandelov, S.; Stimming, U. Trends in the exchange current for hydrogen evolution. *J. Electrochem. Soc.* **2005**, *152* (3), J23−J26.
(36) Kresse, G.; Furthmuller, J. Efficiency of ab-initio total energy calculations for metals and semiconductors using a plane-wave basis set. *Comput. Mater. Sci.* **1996**, *6* (1), 15−50.
(37) Kresse, G.; Furthmuller, J. Efficient iterative schemes for ab initio total-energy calculations using a plane-wave basis set. *Phys. Rev. B: Condens. Matter Mater. Phys.* **1996**, *54* (16), 11169−11186.
(38) Blochl, P. E. Projector augmented-wave method. *Phys. Rev. B: Condens. Matter Mater. Phys.* **1994**, *50* (24), 17953−17979.
(39) Perdew, J. P.; Burke, K.; Ernzerhof, M. Generalized gradient approximation made simple. *Phys. Rev. Lett.* **1996**, *77* (18), 3865−3868.
(40) Tersoff, J.; Hamann, D. R. Theory of the scanning tunneling microscope. *Phys. Rev. B: Condens. Matter Mater. Phys.* **1985**, *31* (2), 805−813.

DOI: 10.1021/acs.nanolett.9b00889
Nano Lett. 2019, 19, 4897−4903